ORIGINAL ARTICLE

Ag nanoparticles immobilized on guanidine modified-KIT-5 mesoporous nanostructure: Evaluation of its catalytic activity for synthesis of propargylamines and investigation of its antioxidant and anti-lung cancer effects

Xifang Wang [a], Zhihong Liu [b,*], Mutasem Z. Bani-Fwaz [c], Riadh Marzouki [c,d,e], Ismat H. Ali [c], Attalla F. El-kott [f,g], Fatimah A. Alhomaid [h]

[a] *Department of Medical Oncology, Shaanxi Provincial People's Hospital, Shaanxi, Xi'an 710068, China*
[b] *Department of Critical Care Medicine, Xi'an International Medical Center Hospital, Xi'an 710000, China*
[c] *Department of Chemistry, College of Science, King Khalid University, P.O. Box 9004, Abha 61413, Saudi Arabia*
[d] *Laboratory of Materials, Crystallochemistry and Applied Thermodynamics, Faculty of Sciences of Tunis, University of Tunis El Manar, Tunisia*
[e] *Chemistry Department, Faculty of Sciences of Sfax, University of Sfax, 3038, Tunisia*
[f] *Biology Department, College of Science, King Khalid University, Abha 61421, Saudi Arabia*
[g] *Zoology Department, College of Science, Damanhour University, Damanhour 22511, Egypt*
[h] *Department of Biology, Faculty of Science, Qassim University, Buraydah, Kingdom of Saudi Arabia*

Abstract   The current study involves the novel synthesis of Ag nanoparticles (Ag NPs) decorated biguanidine modified mesoporous silica KIT-5 following post-functionalization approach (KIT-5-bigua-Ag). The tiny Ag NPs were being stabilized over the *in situ* prepared biguanidine ligand. The high surface area material was characterized using advanced analytical methods like Fourier Transformed infrared (FT-IR) spectroscopy, N_2-adsorption–desorption isotherm, Scanning Electron Microscopy (SEM), Transmission Electron Microscopy (TEM), Energy Dispersive X-ray Spectroscopy (EDS), and X-ray Diffraction study (XRD). The material was having large pore cage like structure with pore diameter of 8–10 nm. TEM study displayed the particles size of deposited Ag

* Corresponding author at: Department of Critical Care Medicine,
Xi'an International Medical Center Hospital, Xi'an 710000, China
 E-mail address: liuzhihong0326@sina.com (Z. Liu).
Peer review under responsibility of King Saud University.

NPs were 10–15 nm. The KIT-5-bigua-Ag nanocomposite had a significantly high surface area of 318 m^2/g (BET analysis). Towards the chemical applications of the material, we headed the three-component reaction of aldehydes, amines and alkynes (A^3 coupling) with good to excellent yields (70–98%) of diverse Propargylamines. The catalyst was easily isolable and reused in 8 cycles without any leaching and considerable change in its reactivity. In addition, the KIT-5-bigua-Ag nanocomposite was engaged in biological assays like study of anti-oxidant properties by DPPH mediated free radical scavenging test using BHT as a reference molecule. Thereafter, on having a significant IC50 value in radical scavenging assay, we extended the bio-application of the desired nanocomposite in anticancer study of A549 cell of human lung in-vitro conditions. In the cytotoxicity and anti-human lung studies, the nanocomposite was treated to lung cancer A549 cell line following MTT assay. The cell viability of malignant lung cell line reduced dose-dependently in the presence of KIT-5-biguanidine-Ag nanocomposite. IC50 values of the nanocomposite were observed to be 915.22 µg/mL against A549 cell line. So, these results suggest that KIT-5-bigua-Ag as a novel chemotherapeutic nanocomposite have a suitable anticancer activity against lung cell lines.

1. Introduction

Designing of a competent heterogeneous nanocatalyst involves the selection of appropriate support that can afford to a maximum immobilization of the targeted functions. Ordered mesoporous silica (OMS) materials are one of the best supports being used these days due to several of its unique properties like ordered porosity, considerable pore volume and high surface area, good mechanical and chemical stability, ability to introduce wide variety of functionalizations on the surface, good sensing ability and adsorption properties, ease to separate from the system, excellent reusability, biocompatibility to carry out biomedical applications and catalysts (Scott et al., 2001; Taguchi and Schuth, 2005). Among the OMS materials, the three dimensional cage-type silica having large pores with grown porous structures have been used as efficient support for many types of heterogeneous catalysis. The large pore three dimensional mesoporous materials have advantages over two dimensional by means of providing large number of active sites leading to high absorptions, ability to absorb larger molecules, high diffusion index for the diffusion of the reactants and biomolecules and most importantly, no chances of pore blocking (MacQuarrie et al., 2010). The nanostructures such as SBA-16, SBA-15, and KIT-5 are examples of the silica mesoporous materials which have pores with 3D close-packed cage-type structure (Liu et al., 2009; Cheng-Yu et al., 2009). The KIT-5 OMS, being first introduced by Ryoo et al., has the Fm3m cubic symmetry, significantly large pores, high pore volume and considerably high surface area (Kleitz et al., 2003). These are sufficient reasons for which we selected KIT-5 as an efficient support for the immobilization of Ag nanoparticles to design a nanocomposite for chemical and biological applications.

Among the different noble metal nanoparticles, Ag NPs are relatively cheaper as compared to Au, Pd and Pt (Mostafavi et al., 2018; Ghonchepour et al., 2019; Ghonchepour et al., 2019; Bananezhad et al., 2019). Based on their distinct characteristics the Ag NPs individually find multilayered applications in different arena like health, medicine, animal husbandry, agriculture, household, packaging, optics, electronics and catalysis (Sadjadi et al., 2020; Mohammadi et al., 2020). Nevertheless, due to ultrafine size and strong electrostatic attraction, frequently the NPs are found to undergo self-aggregation which reduces their efficiency considerably. The biomolecular encapsulated nanocomposite creates a polar environment at surface that shelters the incoming noble ions. They sometime get reduced *in situ* by the electron rich oxidisable groups or needs some external reductant to generate metallic NPs. In addition, the organic groups act as protective capping agent. This in turn, prevents the surface NPs to associate and gets stabilized (Staroverov et al., 2009; Veisi et al., 2020; Veisi et al., 2020; Tamoradi et al., 2020; Veisi et al., 2019; Veisi et al., 2019; Veisi et al., 2015).

The unique coalescence of Ag NPs and KIT-5 could introduce a broad range of utility in biological targeting, biological separation, and catalysis. There have been several in vitro and *in vivo* experimental studies on its chemotherapeutic activities as well as clinical trials on the supported Ag NPs (Qiao et al., 2009; Prabhu and Poulose, 2012; Zhu et al., 2013; Liu et al., 2008). Being encouraged by all these results, we wish to report the synthesis, characterizations and applications of novel Ag NP decorated on biguanidine modified KIT-5 (KIT-5-biguanidine-Ag). The biguanidine function acts as an excellent ligand to anchor Ag (I) ions as well as a very good stabilizer of Ag NPs. The as synthesized nanocomposite (Scheme 1) was proved to be an excellent catalyst while studying its activity in the one-pot multicomponent synthesis of Propargylamines by well-known A^3-coupling of aldehydes, amines and alkynes. Towards its bioapplication, we investigated its anti-oxidant properties as well as the cytotoxicity towards human lung cancer cell lines and obtained some outstanding results.

Propargylamines are important structural scaffold in organic synthesis, being used as precursors of several biologically relevant nitrogen-containing heterocycles like pyrrole, oxazole, pyrazole, imidazole, quinolines etc., different potential drug candidates like β-lactams, pargyline, rasagyline, selegiline etc. and natural products (Lauder et al., 2017; Cortezano-Arellano et al., 2018; Peshkov et al., 2012; Chen et al., 2016; Ramesh and Nagarajan, 2013; Rokade et al., 2019). Typical synthesis of propargylamines follows the metal-catalyzed coupling of **a**ldehydes, **a**mines, and **a**lkynes (A^3-coupling) involving C–H activation of alkynes (Veisi et al., 2019). In the current protocol, KIT-5-bigua-Ag nanocomposite catalyzes the reaction efficiently in aqueous medium under heating conditions to afford the corresponding product in good to excellent yields (Scheme 1). Due to easy recoverability of the catalyst, it was recycled in 8 successive runs over this reaction. In earlier literature, there have been several reports on the catalyzed synthesis of propargylamine derivatives. However, accepting all their own merits, we believe still scopes are there to improve the protocol further. The large surface area, good dispersibility of active Ag NPs without significant agglomeration and high physicochemical stability of the KIT-5-bigua-Ag nanocomposite could be the advantageous points behind using this catalyst. Apart from its chemical applications, we decided to explore the material in biological studies.

Lung is a crucial organ in human respiratory system carrying out the transfusion of O$_2$ and CO$_2$ into blood (World Cancer Research Fund and American Institute for Cancer Research, 2007; Thun et al., 2018). Among the various lung disorders, lung cancer is one
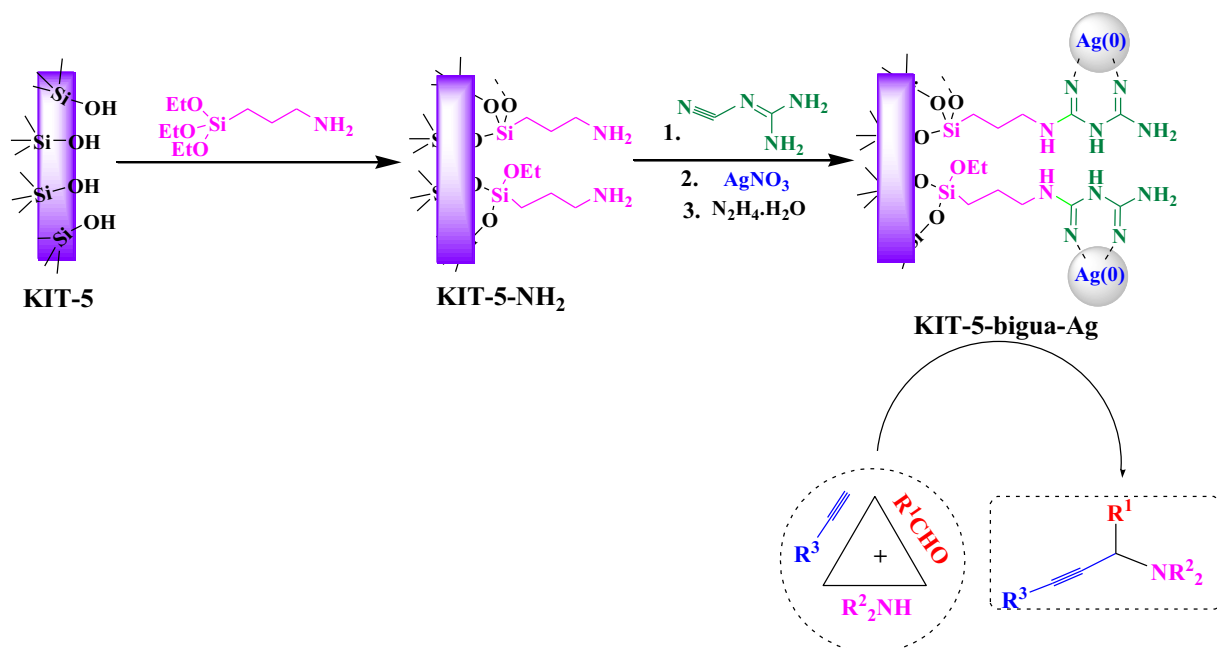
Scheme 1 Post grafting synthesis of KIT-5-bigua-Ag catalyst and its application for the synthesis of propargylamines by A^3-coupling of aldehydes, amines and alkynes.

of the most invasive, metastatic and having severe mortality (Alaoui et al., 2015). Weakness, loss of weight, fatigue, coughing up blood, hoarseness, wheezing, chest pain and dysphagia are the commonest symptoms for lung cancer (Hecht, 2012; Alsharairi, 2019). The conventional treatment protocols for this ailment are chemotherapy, radio therapy, targeted therapy, immunotherapy and surgery (Jones and Baldwin, 2018) which involves fatal side effects , e.g., nerve damage, toxicity, hair loss, diarrhea and mouth sore (Stahl, 2013). Therefore, some alternative or unconventional therapeutic formulations are of high demand. Some of the recent reports have revealed that biomolecules modified NPs exhibit very good anticancer properties (Abdel-Fattah and Ali, 2018; Patil and Kim, 2017; Bisht and Rayamajhi, 2016; Hassanien et al., 2018). Thereby, we have exploited the KIT-5-biguanidine-Ag nanocomposite for the in vitro study of human lung cancer over A549 cell line. Noticeably, we obtained some outstanding results in the antioxidant assay and cytotoxicity studies.

2. Experimental

2.1. Materials and method

The essential chemicals and biosamples were procured from Fluka and Sigma-Aldrich. All the reagents were used directly without any further purifications. In the structural characterizations, FT-IR was recorded over KBr disc in a Bruker VERTEX 80v spectrophotometer. The gas adsorption–desorption isotherms were carried out in a NOVA gas sorption analyzer and a Quantochrome BET surface area analyzer. Morphological and compositional analysis was done over FE-SEM MIRA3 microscope equipped with EDX (TSCAN). The samples were coated with gold atom vapor prior to analysis. A Philips CM10 microscope was used in the TEM analysis, performed at 200 kV operating voltage. The sample was prepared by dispersing it on a carbon coated Cu grid followed by drying. In the analysis of crystallinity, X-ray diffraction study was performed using Co Kα radiation

(λ = 1.78897 Å, voltage 40 keV, current 40 mA) in the scanning range of 2θ = 10 to 80°. A STAT FAX 2100, BioTek, Winooski, USA instrument was used in Microplate Reading.

2.2. Preparation of KIT-5

The mesoporous matrix KIT-5 was prepared following the previously reported method (Veisi et al., 2019). 19.0 g of the triblock copolymer (Pluronic F127) was mixed to 8.5 g HCl (37%) and 192 g H_2O and the mixture was heated at 45 °C for 4 h. Then 19.0 g TEOS was added to it and stirred at same condition for overnight followed by hydrothermal aging at 100 °C for 24 h. The resulting white precipitate was filtered carefully and washed sufficiently with distilled H_2O and dried in air. Finally, the template was removed by calcination at 550 °C for 5 h in air at a ramping rate of 2 °C/min.

2.3. Preparation of KIT-5-bigua

1.0 g of KIT-5 was dispersed in 100 mL anhydrous toluene flask and stirred at ambient temperature for 1 h. 1.0 mL 3-aminoropropyl trimethoxysilane (APTMS) was then added dropwise to the reaction mixture and refluxed for overnight under N_2 atmosphere. After completion, the precipitate was filtered and washed with ethanol (70%) for several times. It was dried subsequently at 60 °C for overnight affording the tripropylamino derivative (KIT-5-NH₂). In the next step, 0.5 g of the KIT-5-NH₂ product was added to 100 mL dry acetonitrile and stirred at 40 °C for 30 min. 3.0 mmol of cyanoguanidine was then added to the reaction mixture and heated at 60 °C for overnight. Finally, the as obtained precipitate was filtered, washed with ethanol (70%) for several times and dried at 60 °C for overnight resulting the KIT-5-bigua (0.58 g) product.

2.4. Preparation of KIT-5-bigua-Ag nanocomposite

0.5 g of the KIT-5-biguanidine composite was adhered into 50 mL acetonitrile and vigorously stirred at 50 °C for 1 h. A 50 mL acetonitrile solution containing 30 mg of AgNO$_3$ was added to the previous suspension very slowly dropwise and subsequently refluxed for 5 h till the formation of Ag(I) complex. Ag(0) NP formation was started *in situ* when hydrazine hydrate (300 µL) was added to it dropwise, as indicated by the change in color to brown–red. The resulting mixture was refluxed for 24 h and finally the grey precipitate was filtered, washed several times with 70% EtOH and dried at 50 °C for overnight in air. The final composite is 0.51 g.

2.5. General procedure for the synthesis of propargylamines catalyzed by KIT-5-bigua-Ag nanocomposite

A mixture of aldehyde (1 mmol), amine (1 mmol), phenyl acetylene (1.2 mmol) and KIT-5-bigua-Ag (15 mg, 0.1 mol%) was heated in water (3 mL) at 80 °C for requisite times. After completion (as monitored by TLC), the catalyst was retrieved by the centrifugation for recycling. The reaction mixture was extracted with ethyl acetate, concentrated and purified through column chromatography (7:3, Hexane/EtOAc).

2.6. Determination of antioxidant property of KIT-5-bigua-Agnanocomposite

DPPH (2,2-diphenyl-1-picrylhydrazyl) was used to study the radical scavenging antioxidant assay of the catalyst. A DPPH solution was prepared in 1:1 aqueous MeOH (39.4 g in 100 mL). Simultaneously, different samples of KIT-5-biguanidine-Ag nanocomposite of variable concentrations (12 samples, 0–1000 µg/mL) were also prepared. The DPPH solution was then added to the different samples of nanocomposite and transferred to an incubator at 37 °C. After 30 min of incubation, the absorbances (A) of the mixtures were measured at 517 nm. MeOH (50 %) and butylatedhydroxytoluene (BHT) were considered as negative and positive controls respectively in the study. The antioxidant property of KIT-5-biguanidine-Ag nanocomposite was determined as

$$\text{Inhibition } (\%) = \frac{\text{Sample } (A)}{\text{Control } (A)} \times 100$$

2.7. Determination of anti-human lung cancer effects of KIT-5-bigua-Ag nanocomposite

The mentioned cell line was cultured at 1×10^5 cell/well in 96-well plates for 24 h at optimal conditions (37 °C, 5% CO$_2$ in humidified incubator). Next, the growth media (10% FBS) was removed and the cells were washed two times with PBS. New maintenance RPMI medium (10% FBS) containing 0.5, 5, 50, 500, and 1000 µg/mL of each compounds was added and the cells were incubated 72 h. Triple wells were analyzed for each concentration and column elution buffer was used as the control. A 10 µL solution of freshly prepared 5 mg/mL MTT in PBS was added to each well and allowed to incubate for an additional 4 h. The media was removed and DMSO was added at 100 µL/well. Plates were shaken gently to facilitate formazan crystal solubilization. The absorbance was measured at 545 nm using a microplate reader. The percentages of cell toxicity and half-maximal inhibitory concentration (IC50) were calculated.

$$\text{Toxicity}\% = (1 - \frac{\text{mean OD of sample}}{\text{mean OD of control}}) \times 100$$

$$\text{Viability}\% = 100 - \text{Toxicity}\%$$

3. Results and discussion

3.1. Catalytic characterizations

The nanocatalyst was synthesized following post-grafting approach over the KIT-5 mesoporous silica and Ag(0) NPs was deposited over the surface functionalized matrix by *in situ* reduction of the chelated Ag(I) ions. The biguanidine moiety was introduced to stabilize the ultrafine Ag(0) NPs by electron donation from the densely located N atoms. The as synthesized material was then characterized using different physicochemical techniques like Fourier Transformed Infrared (FT-IR) Spectroscopy, Field Emission Scanning Electron Microscopy (FESEM), Transmission Electron Microscopy (TEM), N$_2$-adsorption–desorption analysis, Energy Dispersive X-ray Spectroscopy (EDS) and X-ray diffraction (XRD) study.

In order to correlate the stepwise synthesis by organo-ligand functionalization followed by Ag(0) deposition over KIT-5, a comparison between the FT-IR spectra of bare KIT-5, KIT-5-NH$_2$, KIT-5-NH$_2$-bigua and KIT-5-NH$_2$-bigua-Ag materials being recorded in the wavelength region 400–4000 cm^{-1}, presented in Fig. S1. In Fig. S1a, the bands appeared at 460, 793 and 1061 cm^{-1} were related to symmetric stretching, symmetric bending and asymmetric stretching vibrations of Si─O─Si bond respectively. The broad peak appeared at 3433 cm^{-1} was due to the silanol groups (Si─OH). Fig. S1b, the spectra of KIT-5-NH$_2$, depicts some weak peaks at 2840 and 2945 cm^{-1} corresponding to the C─H symmetric and asymmetric stretching frequencies. The broad peak around 3450 cm^{-1}could be the attributed to SiO─H and N─H stretching. The characteristic peaks appeared at 1480 and1610 cm^{-1} in Fig. S1c were due to C─N and C═N stretching frequencies from biguanidine function. The presence of these peaks clearly indicate the successful attachment of cyanoguanidine over KIT-5-NH$_2$. In Fig. S1d, the stretching frequency due to C═N bond was shifted from 1610 to 1605 cm^{-1} which could be attributed to the coordination Ag (0) NPs to biguanidine, implying the immobilization of Ag NPs.

For mesoporous materials, the nitrogen gas adsorption–desorption analysis is an important criteria and the corresponding isotherm has been shown in Fig. 1. Both the bare KIT-5 and KIT-5-bigua-Ag nanocomposite represent a type IV isotherm adjoined with a well-defined H$_2$ hysteresis loop. A sharp capillary condensation occurs at high relative pressure region. In the bare material, the loop closes at 0.4 relative pressure whereas the KIT-5-bigua-Ag hysteresis loop closes at 0.3, corresponding to lower limit of adsorption. The loop width and height decreases in the substituted functional materials as compared to KIT-5 due to shrink in pore volume and cage
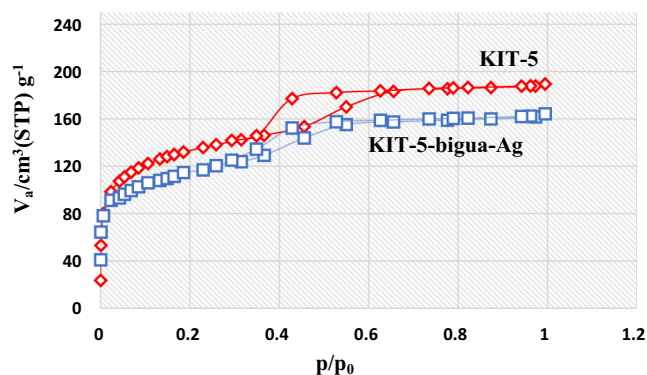
Fig. 1 The N$_2$ adsorption–desorption pattern of the KIT-5 and KIT-5-bigua-Ag nanocomposite.

size. This also is accompanied by the decrease in surface area. The obtained results from N$_2$ ads-des analysis were shown in Table 1.

The structural morphology of the final material has been displayed in Fig. 2. A closer look of the material represents its floppy and cotton like nature. This is obviously due to its high porosity. Due to higher concentration during sampling the particles seem to be agglomerated. The particle diameter is approximately 20 nm. However, no significant appearance is observed in surface engineered KIT-5 material.

The more précised intrinsic morphology could be ascertained from TEM image. The 3D ordered cubic mesostructure is presented in Fig. 3. Interconnected porous channels of KIT-5 matrix can be clearly visible from the image. The black dots represent Ag NPs, being discretely dispersed throughout the surface of functionalized support. Particle size of the Ag NPs were found to be approximately 15–20 nm.

The EDX analysis was performed to evaluate the purity and possible composition of the synthesized KIT-5-bigua-Ag nanocomposite (Fig. 4). It reveals two strong peaks around 2.0–3.0 keV due to Si and Ag as significant elements. Another sharp peak for O appears around 0.5 keV. Some other small bands corresponding to C and N as elements are also observed in the spectrum. The Si represents KIT-5 material, whereas C, N and O represent the organo functions over KIT-5.

Finally, crystalline nature of the KIT-5-bigua-Ag nanocomposite was validated through the X-ray diffraction analysis. Fig. 5, demonstrating the XRD pattern, shows four sharp diffraction peaks and a broad peak. The sharp peaks appeared at $2\theta = 39.1°, 44.1°, 64.2°$ and $77.1°$ represent the Ag face-centred cubic (*fcc*) crystalline phases and corresponds to diffraction on (111), (200), (220) and (311) planes respectively. These characteristic peaks are in close agreement with the standard JCPDS data (JCPDS No. 87-720). The broad peak appeared at $2\theta = 24.5°$ signifies the amorphous silica from KIT-5 base.

Table 1 N$_2$ adsorption-desorption analysis summarize of KIT-5 and KIT-5-bigua-Ag samples.

Sample	V$_p$ (cm^3.g^{-1})	S$_a$ (m^2.g^{-1})	D$_p$ (nm)
KIT-5	116.12	572.12	5.62
KIT-5-bigua-Ag	79.34	318.15	3.89
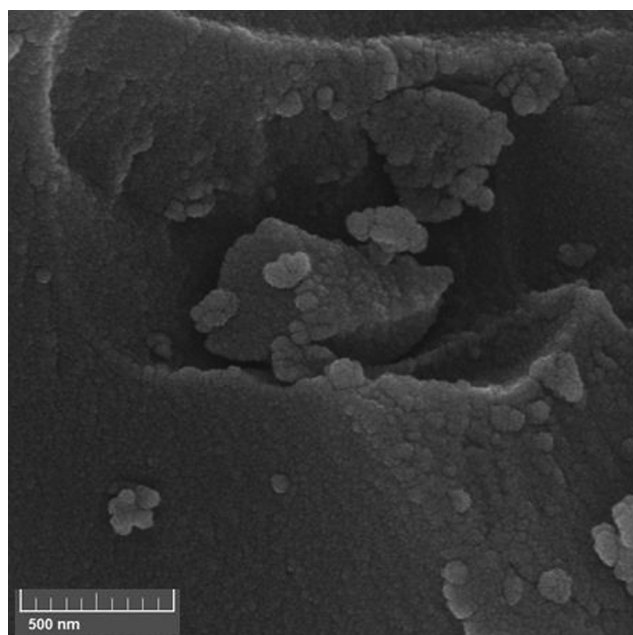
Fig. 2 The SEM image of KIT-5-bigua-Ag nanocomposite.
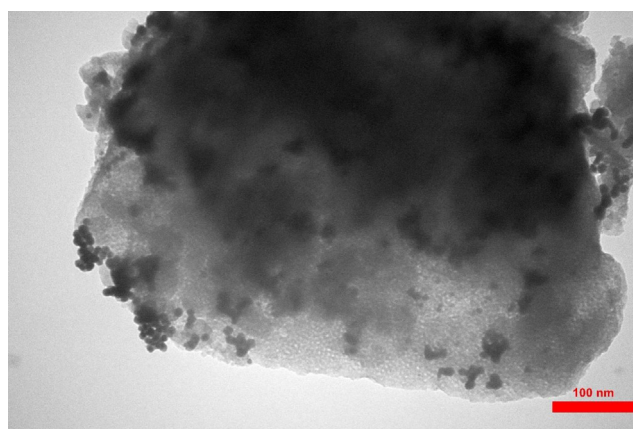
Fig. 3 TEM images of the KIT-5-bigua-Ag nanocomposite.
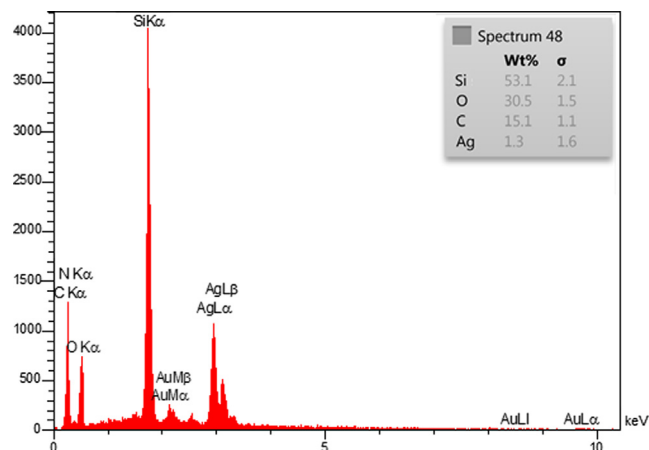
Fig. 4 EDX spectrum of the KIT-5-bigua-Ag nanocomposite.
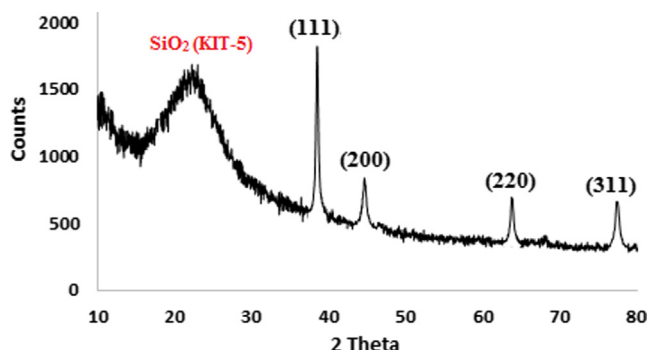
Fig. 5 XRD pattern of the KIT-5-bigua-Ag nanocomposite.

3.2. Catalytic application data analysis

After the meticulous characterizations of KIT-5-bigua-Ag nanocomposite, we turned our attention to explore its catalytic efficiency. We targeted the one-pot three component synthesis of propargylamines by coupling phenyl acetylene, aldehydes and amines, commonly known as A^3 coupling. At the outset, standardization of reaction conditions appeared important and thereby a probe reaction between phenyl acetylene, benzaldehyde and morpholine was chosen. A series of experiments were conducted over the reaction by varying different conditions like solvent, temperature and catalyst load. The results have been documented in Table 2. We started the optimizations with the three substrates in (1.1:1:1) molar ratio in water (3 mL) under heating conditions. There was no product at all in the absence of catalyst (Table 2, entry 1). Using a variable

load, we obtained a quantitative yield in presence of 0.1 mol % of catalyst at 80 °C (entries 3–5 and 13). At lower temperature only a moderate yield was obtained (entry 2). Now, continuing with the 0.1 mol% catalyst, a screening of solvent of variable polarity was carried out under boiling conditions (entries 6–10) and found water as the best one, in terms of eco-friendliness too. Only a poor yield was obtained in solvent-less condition (entry 11). Again, to compare the competence of our catalyst, we used bare KIT-5 and Ag NPs as catalyst in the reaction under otherwise best conditions (entries 14–15). But KIT-5 afforded pore poor yields and Ag NPs yielded moderately. There was high probability of Ag NPs to agglomerate and thereby reducing the catalytic efficiency. Hence, the best conditions for the probe reaction were obtained using 0.1 mol% of KIT-5-bigua-Ag nanocomposite catalyst in water at 80 °C (Table 1, entry 3).

The immediate next endeavor was to find the scopes and generality of those optimized conditions. Thereby, a wide variety of aldehydes and amines were reacted with alkynes to have a library of propargylamines. The results have been shown in Table 3 (entries 1–20). Except the aromatic amines (entry 16), all the aliphatic amines reacted fruitfully regardless the nature of aldehydes. Vis-a-vis, all the aromatic, heteroaromatic and aliphatic aldehydes were highly compatible under the reaction conditions. We also took chance to involve aliphatic alkynes (1-octyne) in the reaction, in addition to phenyl acetylenes and they responded well too (entries 17–20). All the reactions were highly productive with good turnover frequencies (TOF) and turnover numbers (TON).

In sustainable green heterogeneous catalysis, the simplistic isolation of catalyst and its recycle is a crucial factor. Hence, we exploited our catalyst in the probe reaction. After comple-

Table 2 The control experiments towards the optimization of reaction conditions over KIT-5-bigua-Ag nanocatalyst.[a]

Entry	Catalyst (mol%)	Solvent	T (°C)	Time (h)	Yield (%)[b]
1	–	H_2O	50	24	–
2	KIT-5-bigua-Ag (0.1)	H_2O	50	10	60
3	KIT-5-bigua-Ag (0.1)	H_2O	80	8	98
4	KIT-5-bigua-Ag(0.06)	H_2O	80	10	50
5	KIT-5-bigua-Ag (0.03)	H_2O	80	24	50
6	KIT-5-bigua-Ag (0.1)	CH_2Cl_2	70	24	30
7	KIT-5-bigua-Ag (0.1)	DMF	100	10	60
8	KIT-5-bigua-Ag (0.1)	EtOH	80	10	50
9	KIT-5-bigua-Ag (0.1)	Toluene	100	8	98
10	KIT-5-bigua-Ag (0.1)	CH_3CN	70	10	65
11	KIT-5-bigua-Ag (0.1)	–	100	10	25
12	KIT-5-bigua-Ag (0.1)	H_2O	100	8	98
13	KIT-5-bigua-Ag (0.12)	H_2O	80	8	98
14	KIT-5 (0.1)	H_2O	80	24	<10
15	Ag NP (0.1)	H_2O	80	12	74

[a]Reaction conditions: Benzaldehyde (1.0 mmol), phenylacetylene (1.1 mmol), morpholine (1 mmol), KIT-5-biguanidine-Ag, solvent (3.0 mL).
[b]Yields are based on ^1H NMR.

Table 3 The KIT-5-bigua-Ag nanocatalyzed A^3-coupling reaction.[a]
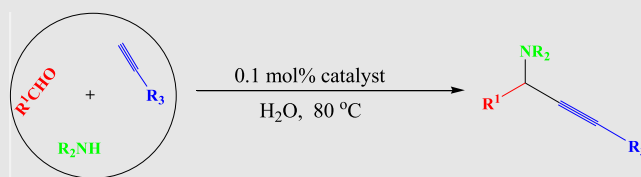
Entry	R^1	Amine	R^3	Yield (%)[b]	TOF (h^{-1})[c]	TON (h^{-1})[d]
1	Ph	Morpholine	Ph	98	122	980
2	4-ClC$_6$H$_4$	Morpholine	Ph	96	120	960
3	3-ClC$_6$H$_4$	Morpholine	Ph	95	118	950
4	4-BrC$_6$H$_4$	Morpholine	Ph	96	120	960
5	4-OHC$_6$H$_4$	Morpholine	Ph	90	112	900
6	4-MeC$_6$H$_4$	Morpholine	Ph	90	112	900
7	4-OMeC$_6$H$_4$	Morpholine	Ph	85	106	850
8	2-Thenyl	Morpholine	Ph	90	112	900
9	2-Furfuryl	Morpholine	Ph	85	106	850
10	Cyclohexyl	Morpholine	Ph	85	106	850
11	C$_3$H$_7$	Morpholine	Ph	80	100	800
12	Ph	Piperidine	Ph	96	120	960
13	Ph	Pyrrolidine	Ph	96	120	960
14	Ph	Diethyl	Ph	90	112	900
15	Ph	Dibenzyl	Ph	85	106	850
16	Ph	Aniline	Ph	0	0	0
17	Ph	Morpholine	n-C$_6$H$_{13}$	85	106	850
18	Ph	Piperidine	n-C$_6$H$_{13}$	75	93	750
19	4-ClC$_6$H$_4$	Morpholine	n-C$_6$H$_{13}$	85	106	850
20	4-OMeC$_6$H$_4$	Morpholine	n-C$_6$H$_{13}$	70	87	700

[a]Reaction conditions: Aldehyde (1.0 mmol), amine (1 mmol), alkyne (1.1 mmol), KIT-5-bigua-Ag (15 mg, 0.1 mol%), water (3.0 mL), 80 °C, 8 h.
[b]Yields are based on 1H NMR.
[c]TOF, turnover frequencies (TOF = (Yield/Time)/Amount of catalyst (mol).
[d]TON, turnover number (TON = Yield/Amount of catalyst (mol).

tion of the first cycle, the catalyst was retrieved from the reaction mixture using centrifuge and it was then regenerated by successive cleaning with H$_2$O and EtOH and dried at 80 °C for 1 h. Noticeably, we recycled the catalyst for 8 successive times without considerable change in its activity (Fig. 6). The high recoverability indicates its robustness and a reason to high TOF and TON in the catalytic process.

We also investigated the true heterogeneous nature of our catalyst by hot filtration test. In the catalytic process, when the reaction yield reached 65% in halfway of the reaction
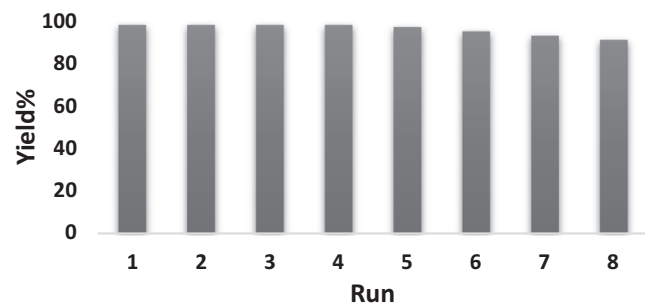
Fig. 6 The reuse of KIT-5-bigua-Ag nanocomposite.

(4 h), the catalyst was separated from the reaction mixture and the catalyst-free reaction was allowed to continue. Amusingly, after 4 h reaction time, there was no further development in the reaction yield. Moreover, the reaction filtrate was studied by ICP-OES analysis. But there was hardly any trace of silver being leached out. This justified the heterogeneity of our catalyst. There have been abundant reports being published over this reaction. The uniqueness of our devised protocol has been validated by comparing some of the previous results with the current one, as shown in Table 4. The results clearly indicate the superiority of our work.

3.3. Antioxidant, cytotoxicity and anti-human lung cancer potentials of KIT-5-bigua-Ag nanocomposite

In this study, the concentration-dependent DPPH radical scavenging effect of KIT-5-biguanidine-Ag nanocomposite was analyzed with respect to a standard molecule (BHT). The interaction between KIT-5-bigua-Ag nanocomposite and DPPH might have occurred by transferring electrons and hydrogen ions (Mahdavi et al., 2019). The scavenging capacity of the KIT-5-bigua-Ag nanocomposite and BHT at different concentrations, expressed in terms of percentage inhibition, has been plotted in Fig. 7. The corresponding IC$_{50}$ values of

Table 4 A catalytic comparison showing the efficiency of current research in the A^3 coupling (entry 12, Table 2).

Entry	Reaction conditions	Temp. (°C)	TOF(h^{-1})	Ref.
1	KIT-5-bigua-Ag, H$_2$O	80	122	This work
2	AgI, H$_2$O, N$_2$	100	3.3	(Srinivasa et al., 2013)
3	Ag NPs, PEG	100	1.92	(Sreedhar et al., 2010)
4	Ag-NaY, neat	100	0.97	(Lakshmi Kantam et al., 2008)
5	Ag-CIN-1,H$_2$O	40	2.72	(Islam et al., 2016)
6	ZnO-IL/Ag, H$_2$O, 3 h	Reflux	51.1	(Samai et al., 2010)
7	PS-NHC-Ag(1),solvent	R.T	4	(Maggi et al., 2008)
8	g-C$_3$N$_4$/Ag(0), EtOH : H$_2$O, microwave	80	245	(Nasrollahzadeh et al., 2015)
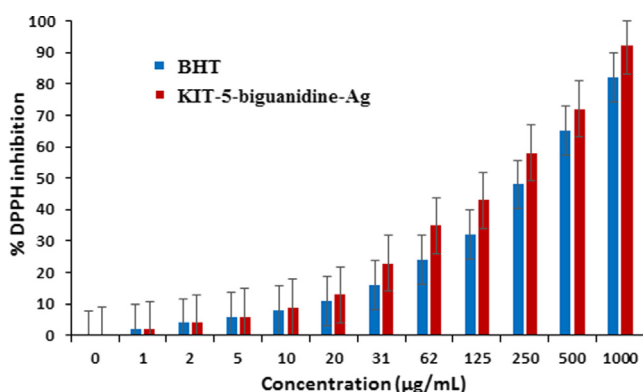
Fig. 7 The antioxidant properties of KIT-5-bigua-Ag nanocompositeand BHT against DPPH. ($p \leq 0.01$).
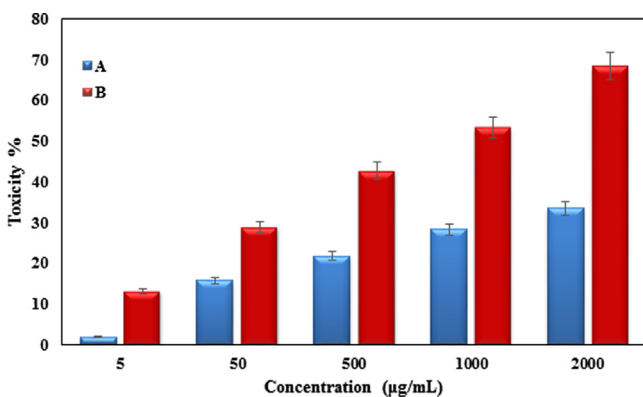
Fig. 8 The anti-human lung cancer properties (Toxicity (%)) of (a) KIT-5-bigua and (b) KIT-5-bigua-Ag nanocomposite (Concentrations of 0–2000 µg/mL) against A549 cell line.

BHT and KIT-5-bigua-Ag nanocomposite were found 274 and 182 µg/mL, respectively.

In the recent research, the treated cells with several concentrations of the present of KIT-5-biguanidine and KIT-5-bigua-Ag nanocomposite were examined by MTT test for 72 h regarding the cytotoxicity properties on A549. The absorbance rate was determined at 545 nm, which indicated extraordinary viability on A549 cell line even up to 2000 µg/mL nanocom-

Table 5 The IC50 of KIT-5-bigua and (b) KIT-5-bigua-Ag nanocomposite against A549 cell line.

	KIT-5-bigua	KIT-5-bigua-Ag
IC50 (µg/mL)	> 2000	915.22

posites (Fig. 8). The results showed, the viability of them reduced dose-dependently in the presence of KIT-5-bigua-Ag nanocomposite. The IC50 of KIT-5-biguanidineand KIT-5-bigua-Ag nanocomposite were > 2000 and 915.22 µg/mL against A549 cell line, respectively (Table 5).

The anticancer potentials of KIT-5-bigua-Ag nanocomposite against human lung cancer cell lines are linked to their antioxidant properties. Several different studies have revealed the strong antioxidant materials such as Ag nanoparticles significantly reduces the volume of tumors by removing free radicals (Mahdavi et al., 2019; Beheshtkhoo et al., 2018; Sangami and Manu, 2017). Our successful effort in exploiting KIT-5-bigua-Ag nanocomposite in lung cancer studies will definitely enlighten the future studies in this arena.

4. Conclusion

In summary, we have been able to synthesize an Ag NPs fabricated organoligand functionalized mesoporous silica nanocomposite (KIT-5-bigua-Ag). The structural features were analyzed through a wide range of analytical techniques. The material was catalytically explored in the one-pot green synthesis of propargylamines by A^3 coupling affording excellent yields. The catalyst was additionally reused for 8 cycles without considerable loss of its activity. Durability of the catalyst was justified by heterogeneity and leaching studies too. The nanocomposite was also explored biologically in the antioxidant and anticancer assays. In the cytotoxicity and anti-human lung studies, the nanocomposite was treated to lung cancer A549 cell line following MTT assay. The cell viability of malignant lung cell line reduced dose-dependently in the presence of KIT-5-bigua-Ag nanocomposite. IC50 values of the nanocomposite were observed to be 915.22 µg/mL against A549 cell line. The outstanding results showed by the developed nanocomposite, could be highly promising in cancer management in near future.

Declaration of Competing Interest

The authors declare that they have no known competing financial interests or personal relationships that could have appeared to influence the work reported in this paper.

Acknowledgements

Appendix A. Supplementary material

Supplementary data to this article can be found online at https://doi.org/10.1016/j.arabjc.2021.103548.

References

Abdel-Fattah, W.I., Ali, G.W., 2018. J. Appl. Biotechnol. Bioeng. 5 (2), 00116.

Alaoui, H.L., Hassan, O., Yang, Y.-W., Buchanan, P., 2015. Biochim Biophys Acta. 1856 (2), 189–210.

Alsharairi, N.A., 2019. Nutrients 11, 725.

Bananezhad, B., Islami, M.R., Ghonchepour, E., Mostafavi, H., Tikdari, A.M., Rafiae, H.R., 2019. Polyhedron 162, 192–200.

Beheshtkhoo, N., Kouhbanani, M.A.J., Savardashtaki, A., et al, 2018. Appl. Phys. A 124, 363–369.

Bisht, G., Rayamajhi, S., 2016. Nanobiomedicine 3, 1–11.

Chen, M.-W., Wu, B., Chen, Z.-P., Shi, L., Zhou, Y.-G., 2016. Org. Lett. 18, 4650–4653.

Cheng-Yu, W., Ya-Ting, H., Chia-Min, Y., 2009. Micropor. Mesopor. Mater. 117, 249–256.

Cortezano-Arellano, O., Hernández-Gasca, M.A., Ángeles-Beltrán, D., NegrónSilva, G.E., Santillan, R., 2018. Tetrahedron Lett. 59, 2403–2406.

Ghonchepour, E., Islami, M.R., Bananezhad, B., Mostafavi, H., Tikdari, A.M., 2019. Compt. Rend. Chim. 22 (1), 84–95.

Ghonchepour, E.M., Islami, R., Tikdari, A.M., 2019. J. Organometal. Chem. 883, 1–10.

Hassanien, R., Husein, D.Z., Al-Hakkani, M.F., 2018. Heliyon 12, e01077.

Hecht, S.S., 2012. Int. J. Cancer. 131, 2724–2732.

Islam, M.M., Roy, A.S., Islam, S.M., 2016. Catal. Lett. 146, 1128–1138.

Jones, G.S., Baldwin, D.R., 2018. Clin. Med. 18, 41–46.

Kleitz, F., Liu, D., Anilkumar, G.M., Park, I.-S., Solovyov, L.A., Shmakov, A.N., Ryoo, R., 2003. J. Phys. Chem. B 107, 14296–14300.

Lakshmi Kantam, M., Laha, S., Yadav, J., Bhargava, S., 2008. Tetrahedron Lett. 49, 3083–3086.

Lauder, K., Toscani, A., Scalacci, N., Castagnolo, D., 2017. Chem. Rev. 117, 14091–14200.

Liu, M.-C., Chang, C.-S., Chan, J.C.C., Sheu, H.-S., Cheng, S., 2009. Micropor. Mesopor. Mater. 121, 41–51.

Liu, C.H., Zhou, Z.D., Yu, X., Lv, B.Q., Mao, J.F., Xiao, D., 2008. Inorg. Mater. 44, 291–295.

MacQuarrie, S., Nohair, B., Horton, J.H., Kaliaguine, S., Crudden, C. M., 2010. J. Phys. Chem. C 114, 57–64.

Maggi, R., Bello, A., Oro, C., Sartori, G., Soldi, L., 2008. Tetrahedron 64, 1435–1439.

Mahdavi, B., Paydarfard, S., Zangeneh, M.M., Goorani, S., Seydi, N., Zangeneh, A., 2019. Appl. Organometal. Chem. 33, e5248.

Mohammadi, P., Heravi, M.M., Sadjadi, S., 2020. Sci. Rep. 10, 6579–6588.

Mostafavi, H., Islami, M.R., Tikdari, A.M., 2018. Appl. Organometal. Chem. 32, (7) e4384.

Nasrollahzadeh, M., Sajadi, S.M., Maham, M., 2015. RSc Adv. 5, 40628–40635.

Patil, M.P., Kim, G.-D., 2017. Appl. Microbiol. Biotechnol. 101, 79–92.

Peshkov, V.A., Pereshivko, O.P., Van der Eycken, E.V., 2012. Chem. Soc. Rev. 41, 3790–3807.

Prabhu, S., Poulose, E.K., 2012. Int. Nano Lett. 2, 32.

Qiao, R.R., Yang, C.H., Gao, M.Y., 2009. J. Mater. Chem. 19, 6274–6293.

Ramesh, S., Nagarajan, R., 2013. Tetrahedron 69, 4890–4898.

Rokade, B.V., Barker, J., Guiry, P.J., 2019. Chem. Soc. Rev. 48, 4766–4790.

Sadjadi, S., Mohammadi, P., Heravi, M.M., 2020. Sci. Rep. 10, 6535–6544.

Samai, S., Nandi, G.C., Singh, M.S., 2010. Tetrahedron Lett. 51, 5555–5558.

Sangami, S., Manu, M., 2017. Environ. Technol. Innov. 8, 150–163.

Scott, B.J., Wirnsberger, G., Stucky, G.D., 2001. Chem. Mater. 13, 3140–3150.

Sreedhar, B., Kumar, A.S., Reddy, P.S., 2010. Tetrahedron Lett. 51, 1891–1895.

Srinivasa, M., Srinivasua, P., Bhargava, S.K., Lakshmi Kantam, M., 2013. Catal. Today 208, 66–71.

Stahl, M. et al, 2013. Ann. Oncol. 24, 51–56.

(a) Staroverov, S.A., Aksinenko, N.M., Gabalov, K.P., Vasilenko, O. A., Vidyasheva, I.V., Shchyogolev, S.Y.U., Dykman, L.A., 2009. Effect of gold nanoparticles on the respiratory activity of peritoneal macrophages. Gold Bull. 42(2), 153-156; 21. (b) Karimi Ghezeli, Z., Hekmati, M., Veisi, H., 2019. Synthesis of Imatinib-loaded chitosan-modified magnetic nanoparticles as an anti-cancer agent for pH responsive targeted drug delivery. Appl. Organometallic Chem. 33, e4833; (c) Ghorbani-Vaghei, R., Hemmati, S., Hekmati, M., 2016. Pd immobilized on modified magnetic Fe$_3$O$_4$ nanoparticles: Magnetically recoverable and reusable Pd nanocatalyst for Suzuki-Miyaura coupling reactions and Ullmann-type N-arylation of indoles, J. Chem. Sci. 128, 1157–1162; (d) Zhang, Wei, Veisi, Hojat, Sharifi, Reyhaneh, Salamat, Delafarin, Karmakar, Bikash, Hekmati, Malak, Hemmati, Saba, Zangeneh, Mohammad Mahdi, Zhang, Zhiyong, Su, Qiang, 2020. Fabrication of Pd NPs on pectin-modified Fe$_3$O$_4$ NPs: A magnetically retrievable nanocatalyst for efficient C–C and C–N cross coupling reactions and an investigation of its cardiovascular protective effects, Int. J. Biol. Mac. 160, 1252–1262; (e) Entezari, M., Safari, M., Hekmati, M., Hekmat, S., Azin, A., 2014. Modification of carboxylated multiwall nanotubes with benzotriazole derivatives and study of their anticancer activities. Med. Chem. Res. 23, 487–495; (f) Azizian, J., Hekmati, M., Dadras, O.G., 2014. Functionalization of carboxylated multiwall nanotubes with dapsone derivatives and study of their antibacterial activities against E. coli and S. aureus. Orient J. Chem. 30, 667–673; (g) Salehi, M.H., Yousefi, M., Hekmati, M., Balali, E., 2019. In situ biosynthesis of palladium nanoparticles on Artemisia abrotanum extract-modified graphene oxide and its catalytic activity for Suzuki coupling reactions. Polyhedron 165, 132–137; (h) Veisi, H., Karmakar, B., Tamoradi, T., Hemmati, S., Hekmati, M., Hamelian, M., 2021. Biosynthesis of CuO nanoparticles using aqueous extract of herbal tea (Stachys Lavandulifolia) flowers and evaluation of its catalytic activity. Sci. Rep. 11, 1983.

Taguchi, A., Schuth, F., 2005. Micropor. Mesopor. Mater. 77, 1–45.

Tamoradi, T., Veisi, H., Karmakar, B., Gholami, J., 2020. Mater. Sci. Eng. C 107, 110260.

Thun, M.J., Hannan, L.M., Adams-Campbell, L.L., 2018. PLoS Medicine 5, e185.

(a) Veisi, H., Sedrpoushan, A., Faraji, A.R., Heydari, M., Hemmati, S., Fatahi, B., 2015. RSC Adv. 5, 68523–68530; (b) Veisi, H., Safarimehr, P., Hemmati, S., 2019. Mater. Sci. Eng.: C 96, 310–318; (c) Veisi, H., Mohammadi, L., Hemmati, S., Tamoradi, T., Mohammadi, P., 2019. ACS Omega 4, 13991–1400; (d) Veisi, H., Manesh, A.A., Eivazi, N., Faraji, A.R., 2015. RSC Adv. 5, 20098–20107; (e) Maleki, B., Hemmati, S., Sedrpoushan, A., Ashrafi, S.S.,

Veisi, H., 2014. RSC Adv. 4, 40505–40510; (f) Hemmati, S., Mehrazin, L., Pirhayati, M., Veisi, H., 2019. Polyhedron 158, 414–422; (g) Baghayeri, M., Amiri, A., Alizadeh, Z., Veisi, H., Hasheminejad, E., 2018. J. Electroanal. Chem. 810, 69–77.

Veisi, H., Ghorbani, M., Hemmati, S., 2019. Mater. Sci. Eng. C. 98, 584–593.

Veisi, H., Tamoradi, T., Karmakar, B., 2019. New J. Chem. 43, 10343.

Veisi, H., Mirzaei, A., Mohammadi, P., 2019. RSC Adv. 9, 41581.

Veisi, H., Moradi, S.B., Safarimehr, P., 2019. Mater. Sci. Eng. C 100, 445–452.

Veisi, H., Ozturk, T., Karmakar, B., Tamoradi, T., Hemmati, S., 2020. Carbohyd. Polym. 235, 115966.

Veisi, H., Tamoradi, T., Karmakar, B., Hemmati, S., 2020. J. Phys. Chem. Solids 138, 109256.

World Cancer Research Fund and American Institute for Cancer Research, 2007. Food, Nutrition, Physical Activity, and the Prevention of Cancer: A Global Perspective. American Institute for Cancer Research, Washington, DC.

Zhu, M., Wang, C., Meng, D., Diao, G., 2013. J. Mater. Chem. A. 1, 2118–2125.